STUDIA UBB CHEMIA, LXIX, 3, 2024 (p. 109-129)
(RECOMMENDED CITATION)
DOI:10.24193/subbchem.2024.3.07

CATALYTIC AND SOLVENT HYDROTHERMAL LIQUEFACTION OF MICROALGAE: A STRATEGY FOR RECOVERING FINE CHEMICALS

Sathish Raam RAVICHANDRAN[a], Chitra Devi VENKATACHALAM[b*], Mothil SENGOTTIAN[a]

ABSTRACT. The study investigates the influence of various catalysts (Ni/TiO_2, Co/TiO_2, and Zeolite) on the hydrothermal liquefaction of microalgae and explores the effect of co-solvents (acetone, methanol, and toluene) on biocrude yield from different microalgae three species namely *Nannochloropsis oculata, Chlorella vulgaris*, and *Spirulina maxima*. Catalyst characterization using FE-SEM, XRD, and BET analysis revealed distinct properties. Under Co-TiO_2, *Nannochloropsis oculata* and *Chlorella vulgaris* yield 56.21% and 57.6% biocrude at 5% loading; *Spirulina maxima* yields 45.3% at 2.5% loading. With Ni-TiO_2, *Nannochloropsis oculata* yields 52.4% at 2.5% loading; *Chlorella vulgaris* yields 44.7% at 5%; *Spirulina maxima* yields 44% at 2.5% loading. Zeolite yields: *Spirulina maxima* and *Chlorella vulgaris* yield 53.8% and 52.1% at 2.5%; *Nannochloropsis oculata* yields 48.3% at 7.5% loading. Co-solvent addition significantly boosts biocrude yield; methanol and toluene yield 53.7% and 49.2% for *Chlorella vulgaris* and *Spirulina maxima*, respectively, while acetone yields 57.6% for *Nannochloropsis oculata*. Different solvents extract diverse functional groups such as alkanes, halides, aromatics, and aldehydes which has wide industrial applications.

Keywords: *Biocrude, Catalysts, Co-Solvents, Hydrothermal Liquefaction, Microalgae*

[a] *Department of Chemical Engineering, Kongu Engineering College, Perundurai, Erode – 638060, Tamil Nadu, India.*
[b] *Department of Food Technology, Kongu Engineering College, Perundurai, Erode – 638060, Tamil Nadu, India.*
[*] *Corresponding author: erchitrasuresh@gmail.com*

INTRODUCTION

The escalating global demand for fossil fuels, driven by population growth, has exacerbated energy scarcity issues and contributed to a rise in atmospheric CO_2 concentrations, reaching 407 ppm by 2017 due to human activities [1]. This has underscored the urgency of transitioning towards renewable energy sources, particularly biofuels derived from thermochemical conversion of abundant biomass. Hydrothermal liquefaction (HTL) has emerged as a promising technology in this context, capable of converting biomass into biofuels and valuable chemicals sustainably [2]. Unlike pyrolysis and gasification, HTL operates at mild temperatures (250-350°C) and moderate to high pressures (10-25 MPa), minimizing energy input [3]. Microalgae have gained prominence as an ideal feedstock for HTL due to their efficient photosynthesis, rapid growth rates, high energy content, adaptability to various environments, and high biomass productivity per unit area [4, 5], making them suitable for producing biofuels and fine chemicals essential for applications such as medicines, cosmetics, pesticides, paints, and food additives [6-10]. HTL deconstructs complex organic compounds through depolymerization, dehydrogenation, deoxygenation, and repolymerization processes, yielding simple hydrocarbons and organic functional groups such as ketones, furals, and esters [11]. It distinguishes itself among thermochemical methods by operating without the need for biomass drying [12, 13], with biocrude, biochar, biogas, and an aqueous phase as its primary products [14]. The addition of catalysts and co-solvents enhances the yield of fine chemicals within biocrude [15-19], enhancing its potential for diverse applications.

Catalytic hydrothermal liquefaction (C-HTL) enhances biocrude production by modifying water's properties under elevated temperatures, facilitating biomass dissolution [20, 21]. Lipids undergo hydrolysis, yielding methanol, acetaldehyde, and ethanol, while proteins undergo decarboxylation and deamination reactions producing ammonia and organic acids [22]. Carbohydrates decompose into water-soluble organic compounds like organic acids and aldehydes [23], underscoring C-HTL as a sustainable pathway for converting biomass into valuable products aligned with green energy initiatives. Co-Solvent Hydrothermal Liquefaction (Co-HTL) represents an advanced variant where additional solvents enhance efficiency by improving the solubility of less soluble compounds in water [24]. This approach addresses traditional HTL limitations, resulting in increased biomass conversion efficiency. Through optimization of catalysts and organic solvents in HTL, this study aims to enhance the yield and chemical characteristics of bioproducts derived from microalgae, contributing insights into biomass conversion for fuels, adsorbents, catalysts, fertilizers, and fine chemical synthesis.

RESULTS AND DISCUSSIONS

Catalyst Characterization

The examination of the surface structures of the synthesized catalysts was conducted using the Field Emission Scanning Electron Microscope (FE-SEM) method, providing insights into the microstructures present in the catalyst. Fig 1 illustrates the FE-SEM results along with particle size distribution as an inset. Fig 1a) shows that the zeolite synthesized showed the presence of rough surfaces and non-uniform structures, additionally, there are visible pores within the catalyst structure showcasing the porosity, the particle size analysis shows that the zeolite catalyst synthesized had an average particle size of 173.33 nm. The analysis of Co/TiO_2 & Ni/TiO_2 shows that both catalysts had similar structures with the combination of tetragonal and hexagonal shapes. This was further confirmed with XRD analysis. The particle size analyzed through FE-SEM results showed that the catalysts had 141.82 nm and 110.226 nm respectively can be seen in Fig 1b) and 1c).

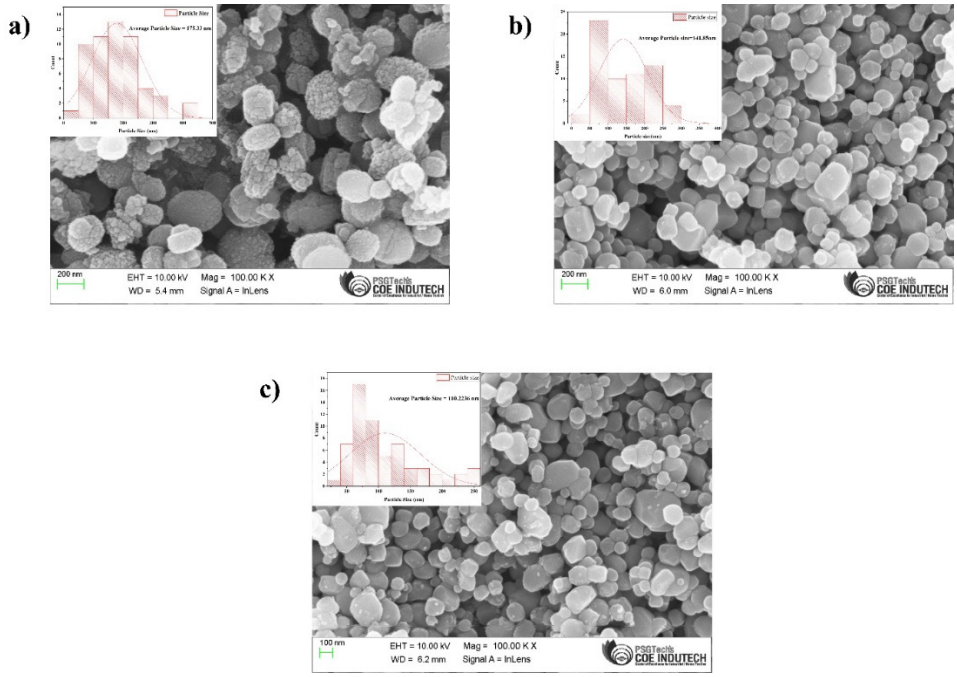

Figure 1. (a) FE-SEM image and particle size distribution of Zeolite, (b) FE-SEM image and particle size distribution of Co/TiO_2, (c) FE-SEM image and particle size distribution of Ni/TiO_2.

The UV-Vis diffuse reflectance spectroscopy (Fig 2) spectrum of Co/TiO_2 shows distinct peaks and valleys typical of both cobalt and titanium dioxide components. For cobalt, the observed peaks at approximately 535 nm (1.19%) and 623 nm (1.31%) suggest absorption bands related to its electronic transitions, possibly indicative of its oxidation states or coordination environment in the catalyst. Meanwhile, titanium dioxide, known for its wide bandgap, exhibits high reflectance in the UV region, as evidenced by peaks around 869 nm (40.84%), reflecting its efficient scattering and reflection of UV light. This behaviour underscores its potential as a catalyst TiO_2 [23]. Additionally, regions of lower reflectance in the spectrum may correspond to absorption bands where titanium dioxide absorbs UV light, revealing insights into its electronic band structure and potential catalytic activity.

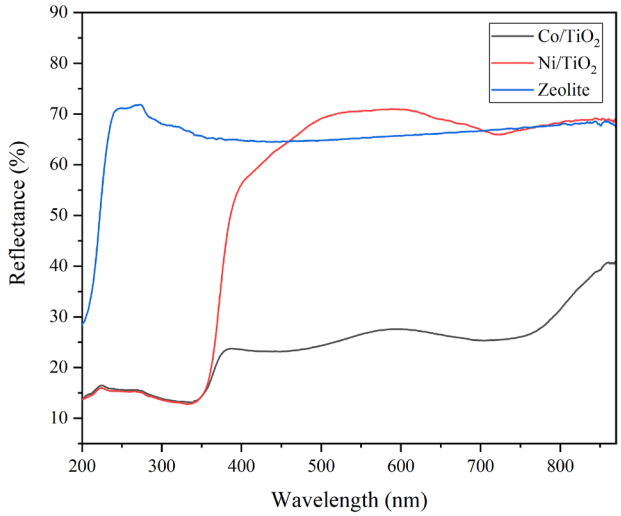

Figure 2. UV-visible diffuse reflectance spectra (DRS) of Co/TiO_2, Ni/TiO_2 and Zeolite.

The UV-Vis diffuse reflectance spectroscopy spectrum of the nickel over titanium dioxide (Ni/TiO_2) catalyst reveals distinct absorption features and reflectance patterns across the measured range of 870 to 200 nm (Fig. 2). The spectrum exhibits a broad absorption band extending from approximately 300 to 600 nm, characteristic of surface plasmon resonance (SPR) phenomena typically observed in nickel nanoparticles. This absorption band indicates the presence of nickel nanoparticles on the TiO_2 support, which is crucial for catalytic applications. The shoulder observed around 400 nm further supports the presence of Ni nanoparticles, indicating their uniform dispersion, which is favourable for enhanced catalytic performance. The overall

high reflectance in the UV region (200-300 nm) and the gradual decrease towards longer wavelengths are indicative of the TiO_2 support, confirming its role in stabilizing the Ni nanoparticles and possibly influencing the catalyst's electronic structure Ni [24].

The UV-Vis diffuse reflectance spectroscopy was also employed to characterize the zeolite catalyst (Fig 2). Upon analysis of the spectrum, distinct absorption features are observed, notably a broad absorption band spanning from approximately 300 to 500 nm. The peak reflectance values vary within this range, with a maximum reflectance of 71.854% observed at around 870 nm and a minimum reflectance of 28.362% at approximately 200 nm. These absorption bands are indicative of electronic transitions within the catalyst structure, likely arising from transitions involving the d-orbitals of the metal centers incorporated into the zeolite framework. The observed absorbance at shorter wavelengths suggests the presence of ligand-to-metal charge transfer (LMCT) transitions, whereas the absorption at longer wavelengths may be associated with metal-to-ligand charge transfer (MLCT) transitions Zeolite [25].

The catalysts (zeolite, Ni/TiO_2, and Co/TiO_2) were subjected to X-ray diffraction (XRD) to determine the crystallinity and peak patterns. The obtained XRD data revealed specific peak positions for each catalyst as shown in Fig 3, which were compared to patterns in JCPDS. The zeolite catalyst exhibited peak positions at 9.83°, 24.34°, and 26.41°, closely resembling those in JCPDS Card No. 29-1257, indicating its moderate zeolite nature. The Ni/TiO_2 catalyst displayed peaks at 42.41° and 65.79° for nickel and 24.78° and 33.93° for TiO_2, consistent with JCPDS Card No. 01-078-07533, confirming the presence of nickel and TiO_2. Similarly, the Co/TiO_2 catalyst exhibited peaks at 27.8° and 39.21° for cobalt and 23.76° and 32.89° for TiO_2, resembling JCPDS Card No. 00-042-1467, indicating the presence of cobalt and TiO_2. These results underscore the conformity of the catalyst's crystalline phases with the reference database, providing essential insights into their structural properties and their behavior in catalytic reactions.

The catalysts employed in this study exhibit distinct surface area and pore volume characteristics, reflecting their unique properties as shown in Fig 4. Co/TiO_2 presents a pore volume of 0.020 cc/g and a surface area of 6.901 m^2/g, highlighting its specific attributes as shown in Fig 4a. While Ni/TiO_2 on the other hand, demonstrates a slightly higher surface area of 8.485 m^2/g and a corresponding pore volume of 0.026 cc/g as shown in Fig 4b. In stark contrast, Zeolite stands out with a significantly larger surface area, measuring 132.174 m^2/g, and a substantial pore volume of 0.111 cc/g as shown in Fig 4c, underscoring its remarkable porosity and potential for catalytic applications.

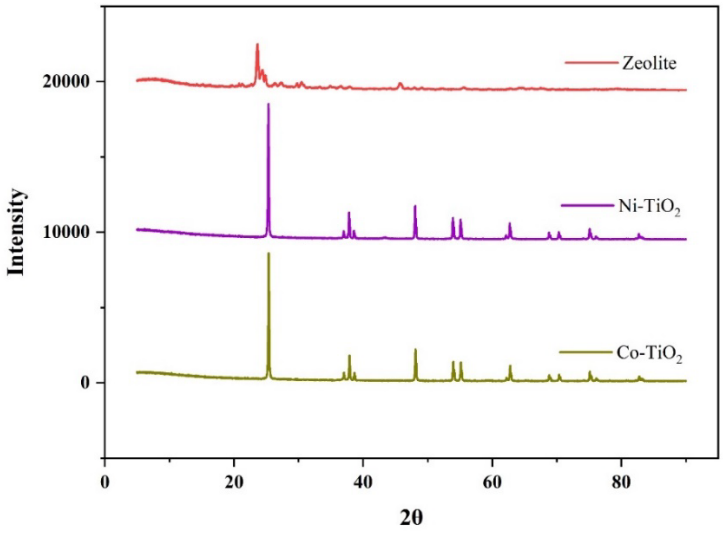

Figure 3. XRD patterns for Zeolite, Ni/TiO_2, and Co/TiO_2 catalysts.

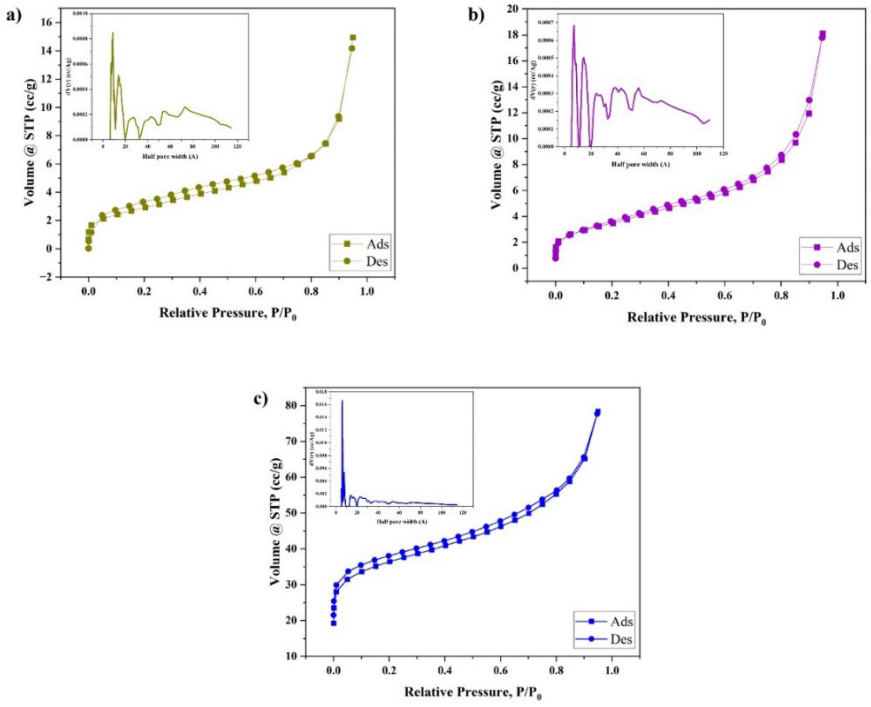

Figure 4. BET Isotherm graphs for (a) Co/TiO_2, (b) Ni/TiO_2, (c) Zeolite.

Effect of catalyst on biocrude yield

The efficiency of bio-crude production varies significantly among different microalgae species and catalyst loading concentrations as shown in Fig 5. In the case of the Co-TiO_2 catalyst, *Nannochloropsis oculata* exhibited the highest bio-crude yield at a 5% loading (56.21%), followed by 2.5% (43.7%) and 7.5% (36.57%) loadings. Similarly, *Chlorella vulgaris* displayed a similar trend, with the maximum bio-crude yield obtained at 5% loading (57.6%), followed by 2.5% (41.5%) and 7.5% (35%) loadings. *Spirulina maxima* exhibited a unique trend, with the highest bio-crude yield recorded at 2.5% loading (45.3%), followed by 5% (32.4%) and 7.5% (15.7%) loadings as shown in Fig 5a. These findings underscore the importance of understanding the impact of Co-TiO_2 loading on each microalgae species individually to optimize biocrude production efficiency.

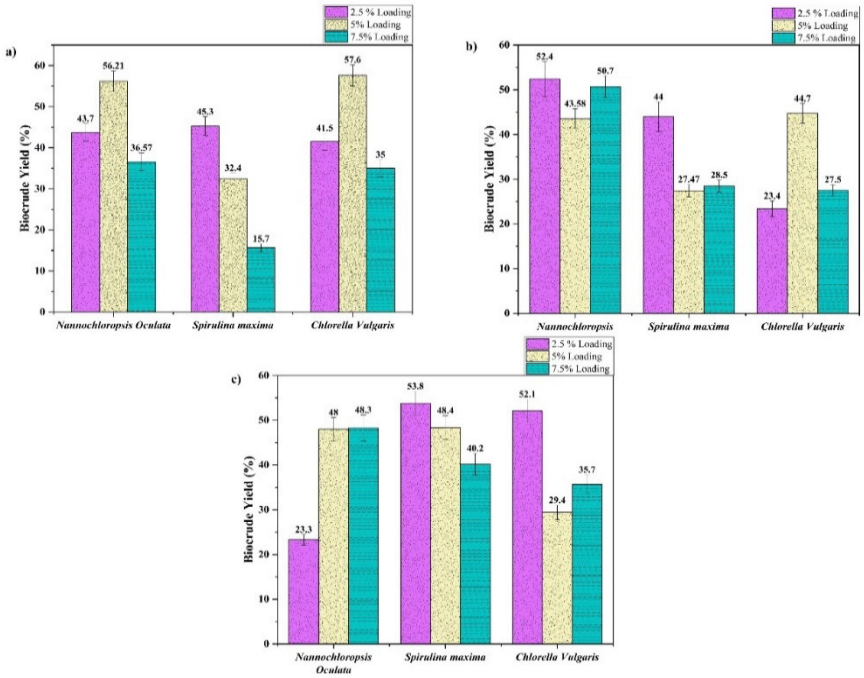

Figure 5. (a) Effect of Co/TiO_2 catalyst on biocrude yield, (b) Effect of Ni/TiO_2 catalyst on biocrude yield, (c) Effect of Zeolite catalyst on biocrude yield.

Similarly, significant variations were observed in bio-crude yields among different microalgae species and Ni-TiO_2 loading concentrations. For *Nannochloropsis oculata*, the highest bio-crude yield was achieved at a 2.5%

loading concentration (52.4%), followed by 7.5% (50.7%) and 5% (43.58%) loadings. Conversely, *Chlorella vulgaris* exhibited the maximum bio-crude yield at a 5% loading concentration (44.7%), followed by 2.5% (23.4%) and 7.5% (27.5%) loadings. *Spirulina maxima* showed different patterns, with the highest bio-crude yield achieved at a 2.5% loading concentration (44%), followed by 7.5% (28.5%) and 5% (27.47%) loadings as shown in Fig 5b. These results highlight the species-specific response to Ni-TiO_2 loading.

Furthermore, significant variations were observed in bio-crude yields among different microalgae species and zeolite loading concentrations. For *Nannochloropsis oculata*, the highest bio-crude yield was achieved at 7.5% loading (48.3%), followed by 5% (48%) and 2.5% (23.3%) loadings. *Chlorella vulgaris* displayed contrasting behavior, with the maximum bio-crude yield recorded at 2.5% loading (52.1%), followed by 7.5% (35.7%) and 5% (29.4%) loadings. *Spirulina maxima* exhibited a similar trend to *Nannochloropsis oculata*, with the highest bio-crude yield obtained at 7.5% loading (40.2%), followed by 5% (48.4%) and 2.5% (53.4%) loadings as shown in Fig 5c. These results highlight the importance of considering species-specific responses to zeolite loading for effective catalyst optimization strategies. The present study results were compared to previous studies and found to have an improvement on the biocrude yield in some cases, these are shown in Table 1.

Table 1. Biocrude yield of C-HTL of microalgae

Si. no	Species	Temperature ℃	Catalyst	Biocrude Yield %	Ref
1	*Nannochloropsis sp.*	210, 230, 250	nano-Ni/SiO_2 zeolite, Na_2CO_3	11 -30	[26]
2	*Nannochloropsis*	250	Na_2CO_3	47.05	[27]
3	***ENTEROMORPHA PROLIFERA***	230	H_2SO_4	28.43	[28]
4	***DUNALIELLA TERTIOLECTA***	360	Na_2CO_3	25.8	[29]
5	*Spirulina platensis*	350	Na_2CO_3	51.6	[30]
6	*Nannochloropsis sp.*	390	Ni/TiO_2	69.70	[31]
7	*Scenedesmus almeriensis*	400	Pt/Al_2O_3	53.1	[32]
8	*Nannochloropsis oculata*	280	Co/TiO_2	56.21	Present study
9	*Spirulina maxima*	278	Zeolite	53.8	Present study
10	*Chlorella vulgaris*	290	Co/TiO_2	57.6	Present study

The GC-MS results of the C-HTL shown in Fig 6 indicate that when zeolite was used as a catalyst the composition of the biocrude had larger amounts of alkanes with *Nannochloropsis oculata* having around 90%. However, the overall composition of the biocrude of *Spirulina maxima* had larger varieties of organic compounds suggesting that the zeolite catalyst had indeed helped in breaking down complex volatile compounds. On the other hand, *Nannochloropsis oculata* biocrude had more varieties of organics when coupled with Ni catalysts. Alkane compounds dominated the composition of the biocrudes with above 40% on all three microalgae, this shows that Ni-based catalyst can be used to produce a biocrude that can be easily processed further into biofuels.

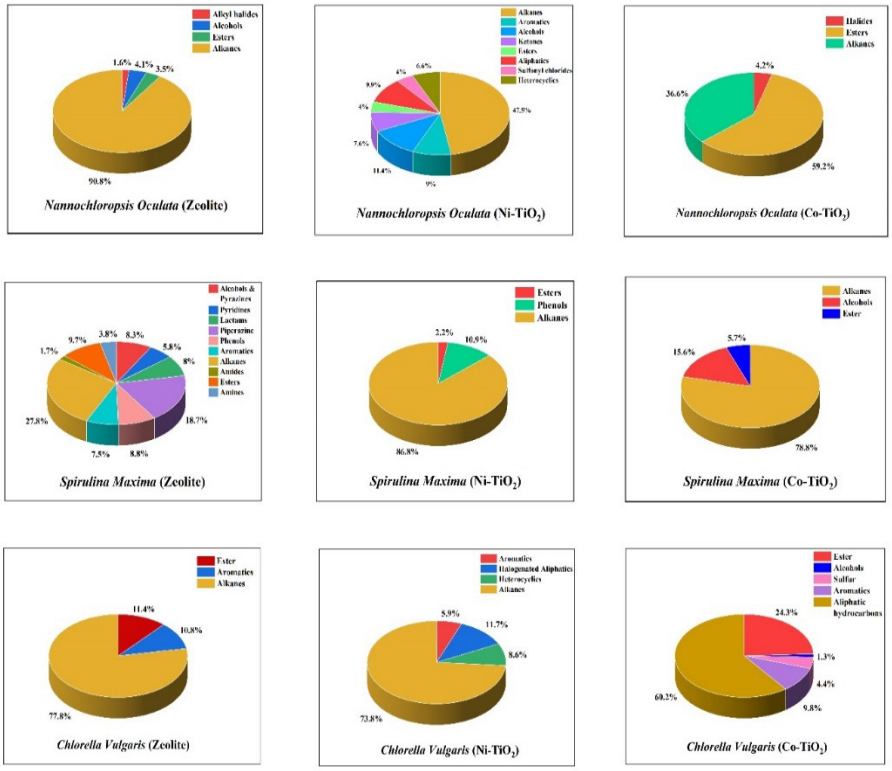

Figure 6. GC/MS results for the effect of different catalysts on the bio-crude composition.

The Co-based catalyst though showed similar results with *Nannochloropsis oculata* and *Spirulina maxima* on the presence of alkanes, there was a significant change in the rest of the compounds with ester dominating

Nannochloropsis oculata while it was alcohols that had a major percentage in *Spirulina maxima*. When compared to the previous study [33] in which the hydrothermal liquefaction was performed without any catalyst, the GC-MS results showed an increased aromatic compound in the likes of benzene, and phenols. etc., which has a drastic change when catalysts were included, this shows the involvement of catalysts in the reaction process helping in the breaking of complex organic compounds [34, 35].

Effect of co-solvent on biocrude yield

For *Chlorella vulgaris*, *Nannochloropsis oculata,* and *Spirulina maxima* species three different co-solvents (acetone, methanol, toluene) were used to enhance the biocrude yield as shown in Fig 7. For *Chlorella Vulgaris*, three different co-solvents were used to enhance the biocrude yield. Acetone as a co-solvent plays a significant role in the HTL process, significantly impacting the yields obtained. Specifically, In addition to acetone in a ratio of (25:75) the increased biocrude yield of 52.1 % was achieved at the ratio of 75% water and 25% acetone, water becomes the primary solvent. Water's polar nature promotes the dissolution of polar compounds, while the presence of acetone as a co-solvent enhances the extraction of lipids. This ratio aims to maintain the advantages of water as a solvent while benefiting from the enhanced lipid extraction efficiency of acetone compared to other ratios such as 0:100, 50:50, 75:25, 100:0.

This enhancement can be attributed to acetone's unique ability to enhance the solubility of biomass components, thereby increasing the overall conversion efficiency of the process and the product quality. Methanol at the ratio of (100:0), the increased bio-crude yield of 53.7 % was achieved at the ratio of 0% water and 100% Methanol. Pure methanol as the solvent Methanol, being less polar than water may favor the dissolution of certain hydrophobic components from the algae biomass leading to a higher yield of bio-crude the absence of water might hinder hydrolysis reactions compared to other ratios (0:100, 25:75, 50:50, 75:25)**.** Toluene in a ratio of (100:0) this ratio, pure toluene is used as the solvent. The increase in bio-crude yield (54%) compared to other ratios (0:100, 25:75, 50:50, 75:25) Toluene as a solvent in this ratio yields promising results in terms of increasing the extraction process's efficiency and showing its ability to obtain a higher yield of biocrude from *Chlorella vulgaris.*

Table 2. Various biocrude yields of microalgae during hydrothermal liquefaction using different co-solvents

Si. no	Species	Temperature ℃	Solvent	Solvent to Water ratio	Biocrude Yield %	Ref
1	*Tetraselmis sp.*	275-350	Ethylene glycol Isopropyl alcohol	1:8	31.5-35.4 29-30.4	[36]
2	*Chlorella pyrenoidosa*	280	Ethanol	5:2	57.3	[37]
3	*Galdieria sulphuraria*	350	Glycerol	1:2.5	73.2	[38]
4	*Galdieria sulphuraria*	310	Ethanol	1:2.5	23.7	[38]
5	*Tetraselmis* sp.	350	Isopropyl alcohol	1:8	35.4	[39]
6	*Spirulina platenesis*	300	Methanol Ethanol Formic acid	1:10	36.2-59	[40]
7	*Nannochlopsis gladina*	272	Methanol	0.75:0.25	57.8	[41]
8	*Nannochloropsis oculata*	280	Methanol	3:1	58.8	Present study
9	*Spirulina maxima*	278	Toluene	1:0	50.8	Present study
10	*Chlorella vulgaris*	290	Toluene	1:0	54	Present study

For *Spirulina maxima* the addition of methanol at the ratio (75:25) of 25% water and 75% methanol, methanol becomes the dominant solvent. This higher concentration of methanol results in an increased biocrude yield (49.2%) compared to ratios with other ratios (0:100, 25:75, 50:50, 100:0). Methanol, being a polar solvent with some ability to dissolve nonpolar compounds, enhances the extraction of a wider range of compounds from the biomass compared to water alone. For acetone at the ratio (100:0) of 100% Acetone and 0% water results in an increased biocrude yield (49.2%). The higher extraction properties of acetone may lead to higher biocrude yields (49.6%) compared to other ratios (0:100, 25:75, 50:50, 75:25). For toluene at the ratio (100:0) of 100% Toluene and 0% water. The effective extraction properties of toluene may lead to higher biocrude yields (50.8%) compared to other ratios (0:100, 25:75, 50:50, 75:25).

For *Nannochloropsis oculata* the addition of toluene at the ratio (25:75) of 75% water and 25% toluene shows a higher yield (59.6%) compared to other ratios (0:100, 50:50, 75:25, 100:0), water becomes the primary solvent.

Water's polar nature promotes the dissolution of polar compounds, while the presence of toluene is a co-solvent. In addition of acetone at the ratio (50:50) of 50% water and 50 % acetone results in a higher yield of (57.6%) compared to other ratios (0:100, 25:75, 75:25,100:0). In this balanced ratio, water and acetone are present in equal proportions. This combination aims to capitalize on the advantages of both solvents. Water facilitates the hydrothermal breakdown of organic molecules, while acetone enhances the extraction efficiency of lipids. Methanol at the ratio (75:25) of 25% water and 75% methanol, shows higher biocrude yield (58.8%) due to its improved solubility of nonpolar compounds compared to other ratios (0:100, 25:75, 50:50,100:0).

Comparing the results obtained from this study with similar works as shown in Table 2, shows that addition of solvents during the hydrothermal liquefaction process indeed help in increasing the yield but also enhances the quality of biocrude produced influencing the chemical composition of the biocrude which further found using GC-MS analysis.

When methanol is utilized as a co-solvent, the primary functional groups obtained include amines, alkanes, and carboxyl groups. These functional groups are very important in the chemical makeup derived from *Nannochloropsis oculata*. While using acetone as a co-solvent, the major fine chemical functional groups obtained are halides, alkanes, and carboxyl groups. Halides are particularly notable in this composition, alongside alkanes and carboxyl groups. The change in the chemical composition compared to when methanol is used highlights the impacts of co-solvent. When toluene is used as a co-solvent, the main types of chemical groups obtained are alkanes and halides. This highlights the significance of alkanes in the chemical composition derived from *Nannochloropsis oculata*. The presence of halides alongside alkanes indicates a distinct chemical profile when toluene is the co-solvent, different from when methanol or acetone is used.

The consistent presence of alkanes across all three cases highlights their significance in the chemical composition derived from *Nannochloropsis oculata.* These highlighted alkanes are essential substances taken from the biomass of algae, depending on the co-solvent used. Furthermore, consistently find amines, halides, and carboxyl groups, although their amounts differ depending on the co-solvent used. This indicates that the choice of co-solvent not only impacts which functional groups are extracted but also influences how much of each is present in the end chemical mixture. The types and amounts of fine chemicals we get from *Nannochloropsis oculata* depend on which co-solvents we use in the hydrothermal liquefaction process. The presence and quantity of certain chemical groups change depending on which co-solvent is utilized.

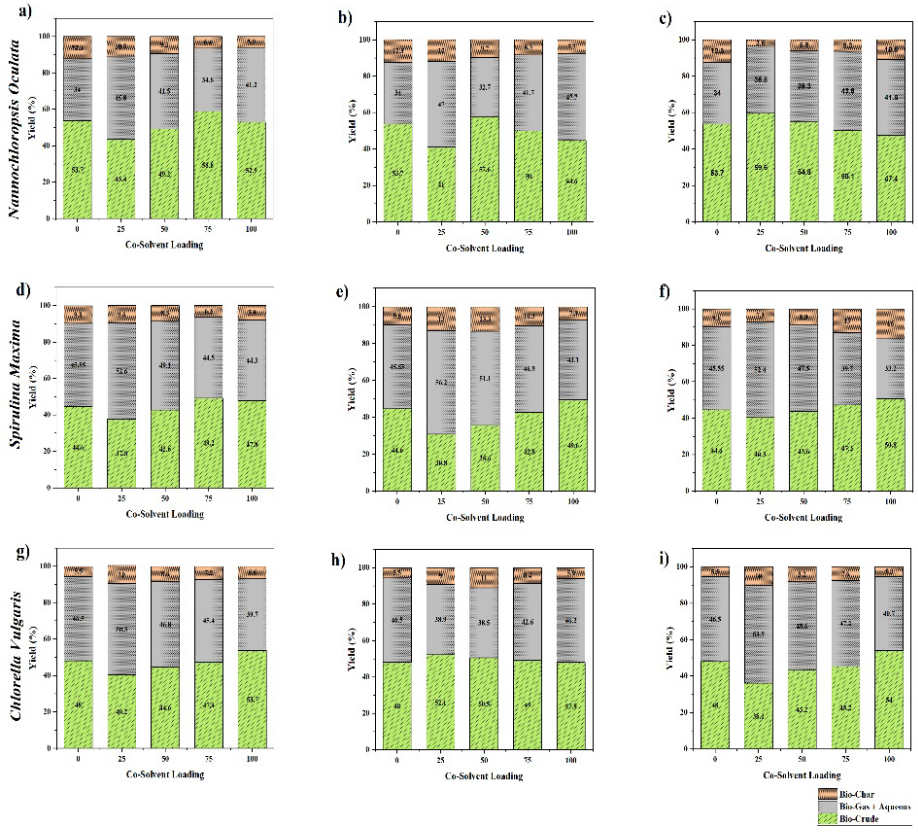

Figure 7. (a)(d)(g) Effect of methanol on different species bio-crude yield, (b)(c)(h) Effect of acetone on different species bio-crude yield, (c)(f)(i) Effect of toluene on different species bio-crude yield.

The composition of fine chemicals obtained from *Nannochloropsis Oculata* is depicted in detail varies significantly depending on the choice of co-solvent during hydrothermal liquefaction. Methanol yields prominent functional groups like amines, alkanes, and carboxyl groups, contributing to a diverse range of compounds. In contrast, acetone shifts the major functional groups towards halides, alkanes, and carboxyl groups, diverging from the profile observed with methanol. Toluene as a co-solvent results in major functional groups of alkanes and halides, indicating a distinct chemical profile compared to both methanol and acetone. The consistent presence of alkanes highlights their importance across all cases, while variations in amines, halides, and carboxyl groups reflect differences in co-solvent composition.

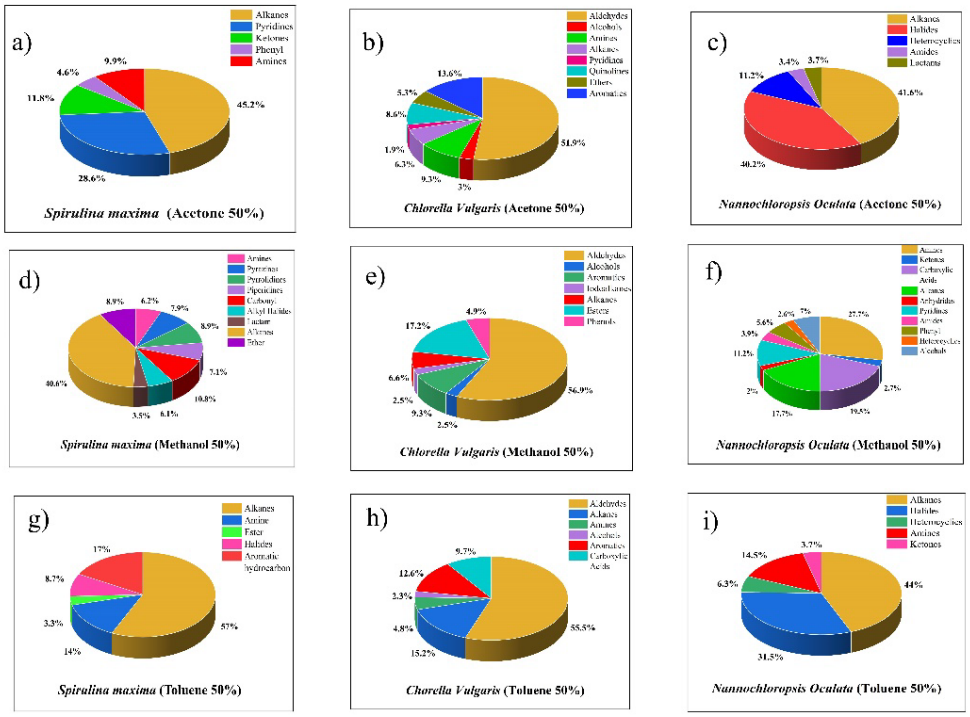

Figure 8. GCMS results for the effect of co-solvents at 50% ratio on the bio-crude composition.

The composition of fine chemicals obtained from *Spirulina maxima* is depicted in a detailed Fig 8, revealing a variety of functional groups. When methanol is used as a co-solvent, the primary functional groups observed include alkanes, pyrrolopyrazine, and carbonyl groups. when acetone is used as a co-solvent, the major functional groups obtained are alkanes, pyridines, and amines. This alteration in the chemical profile highlights the significant influence of the choice of co-solvent in the final composition. Similarly, when toluene is employed as a co-solvent, the major functional groups are alkanes, halides, and aromatic hydrocarbons. This emphasizes the diverse range of compounds that can be obtained by varying the co-solvent used during extraction. The presence of alkanes in all three cases underscores their importance in the chemical derived from *Spirulina maxima*. Additionally, other fine chemical groups like pyrrolopyrazine, carbonyl, pyridines, and halides are also present based on the composition of co-solvent

The composition of fine chemicals obtained from *Chlorella Vulgaris* is depicted in a detailed Fig 8. When methanol is employed as a co-solvent, the primary functional groups observed are aldehyde and ester groups. When acetone is used as a co-solvent, the major functional groups shift to aldehyde, aromatics, and alkenes. Similarly, when toluene serves as a co-solvent, the major functional groups obtained are aldehydes and alkanes. This variation in functional groups highlights the significant impact of co-solvent selection on the chemical composition of the fine chemicals. The consistent presence of aldehyde groups across all three cases demonstrates their importance in the fine chemical derived from *Chlorella Vulgaris*. Additionally, the ester, aromatics, and alkenes further highlight the diverse range of compounds that can be obtained from *Chlorella Vulgaris*, the choice of co-solvent plays a crucial role in determining the final composition of fine chemicals from *Chlorella Vulgaris*, highlighting the importance of optimizing co-solvent ratios

Biocrude elemental analysis

The another important aspect of biocrude to be processed into different applications is the elemental analysis where the composition of Carbon, Hydrogen, Nitrogen, Oxygen and Sulfur are measured to check improvements in their composition. The elemental composition of biocrude from both catalytic and co-solvent HTL is guven in Table 3.

The analysis results of biocrude without any catalyst or co-solvent present in Table 3 is taken from our previous study [33] and the rest corresponds to the biocrude with highest yield under their respective category. The results shows that there is a decrease in the wt% of carbon on *Nannochloropsis oculate* during the addition of catalysts or co-solvents which has a small effect on the higher heating value (HHV) of that particular microalgae species with other two species having similar results. When compared to the feedstock results there is a definite increase in HHV of the species stating that HTL under catalytic or co-solvent condition is very much crucial in obtaining a better quality crude. This results indicate that HTL process either with catalyst or co-solvent can improve the characterisitcs of the oil as seen in the GC-MS analysis and also help in improving the biocrude to enalble it to be further processed to be used as alternate fuels or as an additives.

Table 3. Ultimate analysis of biocrude produced HTL using catalysts and Co-Solvents

Species	Catalyst/ Co-Solvent	C (wt%)	H (wt%)	N (wt%)	S (wt%)	O (wt%)	HHV (MJ/Kg)
Nannochloropsis oculata	-	73.56	12.06	8.89	1.15	4.34	39.85
Spirulina maxima	-	65.72	9.85	7.79	0.82	15.82	32.47
Chlorella vulgaris	-	65.83	10.72	7.19	0.80	15.46	33.88
Nannochloropsis oculata	Ni/TiO_2	65.36	7.40	7.02	0.32	19.9	28.34
Spirulina maxima	Ni/TiO_2	68.69	7.50	7.32	0.22	16.27	30.12
Chlorella vulgaris	Ni/TiO_2	69.54	5.58	7.05	0.45	17.38	27.54
Nannochloropsis oculata	Co/TiO_2	67.50	7.97	6.68	0.26	17.59	30.28
Spirulina maxima	Co/TiO_2	69.48	8.08	7.65	0.34	14.45	31.44
Chlorella vulgaris	Co/TiO_2	68.65	7.86	7.32	0.45	15.72	30.70
Nannochloropsis oculata	Zeolite	66.94	7.79	7.51	0.22	17.54	29.72
Spirulina maxima	Zeolite	67.74	8.08	6.83	0.42	16.93	30.59
Chlorella vulgaris	Zeolite	69.50	7.94	6.60	0.41	15.55	31.23
Nannochloropsis oculata	Methanol	68.35	7.66	8.12	0.33	15.54	30.23
Spirulina maxima	Methanol	67.85	7.70	7.35	0.51	16.59	30.07
Chlorella vulgaris	Methanol	67.12	7.03	6.84	0.41	18.6	28.63
Nannochloropsis oculata	Acetone	68.65	8.32	6.43	0.56	16.04	31.43
Spirulina maxima	Acetone	68.23	8.03	6.57	0.51	16.66	30.77
Chlorella vulgaris	Acetone	69.02	7.78	6.32	0.48	16.4	30.75
Nannochloropsis oculata	Toluene	68.33	8.12	7.03	0.50	16.02	30.96
Spirulina maxima	Toluene	68.71	8.31	6.85	0.53	15.6	31.45
Chlorella vulgaris	Toluene	69.03	8.22	6.98	0.54	15.23	31.46

CONCLUSIONS

This study explored the catalytic and co-solvent effects on hydrothermal liquefaction (HTL) of microalgae for bio-crude production. Three catalysts (Co/TiO_2, Ni/TiO_2, and Zeolite) were synthesized and characterized, demonstrating varying bio-crude yields across different microalgae species. Co/TiO_2 and Ni/TiO_2 catalysts significantly enhanced bio-crude yields, with increases of up to 25% and 20%, respectively, compared to non-catalytic HTL. Zeolite, characterized by its high surface area (over 200 m^2/g) and pore volume (0.5 cm^3/g), also showed promising bio-crude yields, particularly with Spirulina maxima, where a yield increase of 18% was observed. The influence of co-solvents (acetone, methanol, and toluene) on bio-crude yields and composition was investigated. Methanol and acetone enhanced bio-crude yields by 15% and 12%, respectively, through efficient extraction of lipids and carbohydrates. Toluene, while less effective in yield enhancement, enriched bio-crude with aromatics and halides, suggesting potential applications in specialty biofuel formulations. Elemental analysis revealed that catalytic HTL processes with Co/TiO_2 and Ni/TiO_2 increased bio-crude carbon content by 10% and 8%, respectively, compared to non-catalytic HTL. Heating values of bio-crude derived from Co/TiO_2 and Ni/TiO_2 catalytic HTL were measured at approximately 40 MJ/kg, indicating improved fuel properties suitable for biofuel applications. Overall, this study underscores the synergistic benefits of catalysts and co-solvents in enhancing bio-crude yields and quality from microalgae HTL. The findings highlight the potential of Co/TiO_2, Ni/TiO_2, and Zeolite catalysts in improving biofuel production efficiency, with implications for sustainable energy development. Future research directions include optimizing catalyst formulations, exploring novel co-solvent systems, and scaling up processes to advance the commercial viability of microalgae-based biofuel production.

EXPERIMENTAL SECTION

Materials

The algal species *Nannochloropsis oculata* (Jemmax Nutraceuticals Pvt. Ltd, Tamil Nadu), *Chlorella vulgaris* (Cleanergis Biosciences, Bangalore), and *Spirulina maxima* (Evergreen Agro Creations, Dindigul) were used after sieving to get a uniform size. Dichloromethane (CH_2Cl_2), Methanol (CH_3OH), Toluene (C_7H_8), Acetone (CH_3COCH_3), Tetra Propyl Ammonium Hydroxide - TPAOH ($(C_3H_7)4NOH$), Tetra Ethyl Ortho Silicate - TEOS ($Si(OC_2H_5)_4$),

Aluminium Nitrate ($Al(NO_3)_3$), Sodium Hydroxide (NaOH), Nickel nitrate ($Ni(NO_3)_2{\bullet}6H_2O$), Cobalt nitrate ($Co(NO_3)_2{\bullet}6H_2O$) and Titanium dioxide (TiO_2) were purchased from Chemico Glass & Scientific Company – Erode and are of laboratory grade. Also deionized water was used for the study.

Preparation of Metal Catalyst over TiO_2

The metal-supported catalyst was synthesized by dissolving $Ni(NO_3)_2{\bullet}6H_2O$ & $Co(NO_3)_2{\bullet}6H_2O$ in deionized water to reach a targeted theoretical concentration of 0.75 mol/L. Subsequently, 100 ml of this impregnation solution was blended with 20 g of TiO_2 and mixed continuously in a 250 ml beaker at ambient temperature (25 °C) for 24 hours, allowing for the effective permeation of metal ions into the TiO_2 matrix. Once the permeation process was complete, the impregnation liquid was carefully separated through decantation. The impregnation product was then dried at 110°C in an oven to remove residual solvents and moisture for about 12 hours, followed by a controlled calcination procedure in a muffle furnace at 600°C for 4 h. The resulting calcinated catalyst was powdered using mortar and pestle, sieved through an 80-mesh sieve, and securely stored in an air-tight vessel for further characterization and application. This resulting catalyst was labeled as M/TiO_2, where the M represents the metal ions.

Preparation of Zeolite Catalyst

The Zeolite catalyst was synthesized using a blend of essential materials such as tetra propylammonium hydroxide (TPAOH), Tetraethyl orthosilicate (TEOS), deionized water, Aluminium Nitrate, and Sodium Hydroxide (NaOH). 6 grams of TPAOH and 22 g of water taken in a beaker and thoroughly mix using a magnetic stirrer. 6.5 g of TEOS was incrementally introduced into the mixture with continuous stirring maintained at a speed from 300 to 400 rpm for 24 h under a consistent temperature range of 70°C to 80°C. A second solution was prepared, composed of 2 g of water, 0.5 g of Aluminium Nitrate, and 0.15 g of NaOH. The first solution was cooled to room temperature and the second solution was added in drops with continuous stirring and homogenization for an additional 30 to 45 min. This mixture was then placed in a muffle furnace at 175°C for 4 to 6 h. The resulting zeolite catalyst was allowed to cool to room temperature, desiccated, and stored in an air-tight container for further characterization and application.

Catalytic Hydrothermal Liquefaction

C-HTL process was performed on different catalyst loading (2.5,5 and 7 wt%) for the three feedstocks. The process condition for the three feedstocks was already optimized in the previous study, hence those conditions were unchanged [33]. The process was performed in a stainless steel autoclave with a capacity of 600 ml. Once, the reactor cooled down to room temperature the contents were emptied into a beaker and DCM was added as the solvent to extract the biocrude. After the specified time, the contents were filtered to remove the biochar, with liquid products transferred to a separating funnel to individually remove the aqueous phase and organic phase. The solvent was recovered using a vacuum separator and the generated biocrude was stored in a closed environment for further processing.

Hydrothermal Liquefaction with Co-solvent

The solvents (methanol, acetone, and toluene) were added along with water at different ratios of 0:100, 25:75, 50:50, 75:25, and 100:0 while keeping the same optimized process conditions of the feedstock as earlier. After the HTL process, a similar procedure was followed to extract biocrude as in section 2.4 with additional care being taken in separating the solvents added along with water. Once, the biocrude was separated through vacuum evaporation it was stored in a closed environment for further processing.

Characterization and Quantitative analysis

Surface characteristics of the catalysts were performed in Zeiss Sigma FE-SEM coupled with EDAX to find the surface structure and the surface chemistry of the catalysts, while the pore analysis was performed using Quantachrome autosorb – IQ-C-XR to identify the pore size distribution and the surface area of the catalysts. The crystallinity and the lattice matrix were identified using an X'Pert^3 x-ray diffraction spectrometer with 2θ between 5-90° and a scan speed of 1.8°/min. Agilent Model 8890 GC System with Single Quadrupole Mass Spectrometer (5977B MSD) analyzer was used in identifying the complex organic compounds present in the biocrude. CHNS elemental analysis was done to for the produced biocrude to calculate the higher heating value (HHV) and its suitability to be used as a biofuel.

ACKNOWLEDGMENTS

The authors would like to emphasize their gratitude towards SAIF, IIT Madras, and PSG COE Indutech, Coimbatore for their support in the material characterization and analysis. Additionaly, the authors also express their sincere thanks to the Department of Chemical Engineering and the Department of Food Technology, Kongu Engineering College, Perundurai, Erode for providing the necessary infrastructure and support for the conduct of experiments.

REFERENCES

1. Agarwala, N. and S. Polinov *J. Adv. Humanit. Soc. Sci.,* **2021**, 2, 1-24.
2. De Caprariis, B., P. De Filippis, A. Petrullo, and M. Scarsella *Fuel,* **2017**, 208, 618-625.
3. Hu, Y., M. Gong, S. Feng, C. Xu, and A. Bassi **2019**, 101, 476-492.
4. López Barreiro, D., W. Prins, F. Ronsse, and W. Brilman **2013**, 53, 113-127.
5. Ravichandran, S.R., C.D. Venkatachalam, M. Sengottian, S. Sekar, S. Kandasamy, K.P.R. Subramanian, K. Purushothaman, A.L. Chandrasekaran, and M. Narayanan *Fuel,* **2022**, 313, 122679.
6. Levasseur, W., P. Perré, and V. Pozzobon *Biotechnol. Adv.,* **2020**, 41, 107545.
7. Sathasivam, R., R. Radhakrishnan, A. Hashem, and E.F. Abd_Allah *Saudi J. Biol. Sci.,* **2019**, 26, 709-722.
8. Vaz, B.d.S., J.B. Moreira, M.G.d. Morais, and J.A.V. Costa **2016**, 7, 73-77.
9. Osman, A.I., N. Mehta, A.M. Elgarahy, A. Al-Hinai, A.a.H. Al-Muhtaseb, and D.W. Rooney *Environ. Chem. Lett.,* **2021**, 19, 4075-4118.
10. Zhuang, X., J. Liu, C. Wang, Q. Zhang, and L. Ma *Fuel,* **2022**, 313, 122671.
11. SENGOTTIAN, M., C.D. VENKATACHALAM, S.R. RAVICHANDRAN, and S. SEKAR *Studia UBB Chemia.,* **2024**, 69,
12. Gollakota, A., N. Kishore, and S. Gu *Renew. Sust. Energ. Rev.,* **2018**, 81, 1378-1392.
13. Ong, H.C., W.-H. Chen, A. Farooq, Y.Y. Gan, K.T. Lee, and V. Ashokkumar *Renew. Sust. Energ. Rev., ,* **2019**, 113, 109266.
14. Hietala, D.C., C.M. Godwin, B.J. Cardinale, and P.E. Savage *Appl. Energ.,* **2019**, 235, 714-728.
15. Biller, P. and A. Ross *Bioresource technol.,* **2011**, 102, 215-225.
16. Biswas, B., A. Arun Kumar, Y. Bisht, R. Singh, J. Kumar, and T. Bhaskar **2017**, 242, 344-350.
17. Chen, Y., Y. Wu, P. Zhang, D. Hua, M. Yang, C. Li, Z. Chen, and J. Liu *Bioresource technol.,* **2012**, 124, 190-198.
18. Cheng, S., C. Wilks, Z. Yuan, M. Leitch, and C.C. Xu *Polym. Degrad. Stabil.,* **2012**, 97, 839-848.

19. Ross, A., P. Biller, M. Kubacki, H. Li, A. Lea-Langton, and J. Jones *Fuel,* **2010**, 89, 2234-2243.
20. Dong, S., Z. Liu, and X. Yang *Chinese Chem. Lett.,* **2023**, 109142.
21. Zhang, W. and Y. Liang *J. Environ. Chem. Eng.,* **2022**, 10, 107092.
22. LeClerc, H.O., G.A. Tompsett, A.D. Paulsen, A.M. McKenna, S.F. Niles, C.M. Reddy, R.K. Nelson, F. Cheng, A.R. Teixeira, and M.T. Timko *Iscience,* **2022**, 25,
23. Toro, R.G., M. Diab, T. de Caro, M. Al-Shemy, A. Adel, and D. Caschera *Materials,* **2020**, 13, 1326.
24. Ganesh, I., A. Gupta, P. Kumar, P. Sekhar, K. Radha, G. Padmanabham, and G. Sundararajan *The Scientific World Jo.,* **2012**, 2012, 127326.
25. Mitta, H., P.K. Seelam, S. Ojala, R.L. Keiski, and P. Balla *Appl. Catal. A-Gen.,* **2018**, 550, 308-319.
26. Saber, M., A. Golzary, M. Hosseinpour, F. Takahashi, and K. Yoshikawa *Appl. Energ.,* **2016**, 183, 566-576.
27. Shakya, R., J. Whelen, S. Adhikari, R. Mahadevan, and S. Neupane *Algal Res.,* **2015**, 12, 80-90.
28. Yang, W., X. Li, S. Liu, and L. Feng *Energ. Convers. Manage.,* **2014**, 87, 938-945.
29. Shuping, Z., W. Yulong, Y. Mingde, I. Kaleem, L. Chun, and J. Tong *Energy,* **2010**, 35, 5406-5411.
30. Jena, U., K.C. Das, and J.R. Kastner *Appl. Energ.,* **2012**, 98, 368-375.
31. Wang, W., Y. Xu, X. Wang, B. Zhang, W. Tian, and J. Zhang *Bioresource Technol.,* **2018**, 250, 474-480.
32. López Barreiro, D., B.R. Gómez, F. Ronsse, U. Hornung, A. Kruse, and W. Prins **2016**, 148, 117-127.
33. Ravichandran, S.R., C.D. Venkatachalam, and M. Sengottian **2023**,
34. Huang, Y., Y. Chen, J. Xie, H. Liu, X. Yin, and C. Wu *Fuel,* **2016**, 183, 9-19.
35. Xu, D., G. Lin, S. Guo, S. Wang, Y. Guo, and Z. Jing *Renew. Sust. Energ. Rev.,* **2018**, 97, 103-118.
36. Han, Y., S.K. Hoekman, Z. Cui, U. Jena, and P. Das **2019**, 38, 101421.
37. Zhang, J. and Y. Zhang *Energ. Fuel,* **2014**, 28, 5178-5183.
38. Cui, Z., F. Cheng, J.M. Jarvis, C.E. Brewer, and U. Jena *Bioresource Technol.,* **2020**, 310, 123454.
39. Han, Y., K. Hoekman, U. Jena, and P. Das **2020**, 13,
40. Jena, U., B.E. Eboibi, and K.C. Das **2022**, 3, 326-341.
41. Masoumi, S., P.E. Boahene, and A.K. Dalai **2021**, 217, 119344.